Journal of Biomechanics 45 (2012) 2684–2689

Contents lists available at SciVerse ScienceDirect

Journal of Biomechanics

journal homepage: www.elsevier.com/locate/jbiomech
www.JBiomech.com

Quantification of red blood cell deformation at high-hematocrit blood flow in microvessels

Davod Alizadehrad [a], Yohsuke Imai [b,*], Keita Nakaaki [b], Takuji Ishikawa [b], Takami Yamaguchi [a]

[a] Department of Biomedical Engineering, Tohoku University, Japan
[b] Department of Bioengineering and Robotics, Tohoku University, 6-6-01 Aramaki Aza Aoba, Sendai 980-8579, Japan

ARTICLE INFO

Article history:
Accepted 21 August 2012

Keywords:
Microcirculation
Red blood cell deformation
Dense suspension
Numerical simulation

ABSTRACT

The deformation of red blood cells in microvessels was investigated numerically for various vessel diameters, hematocrits, and shear rates. We simulated blood flow in circular channels with diameters ranging from 9 to 50 μm, hematocrits from 20% to 45%, and shear rates from 20 to 150 s^{-1} using a particle-based model with parallel computing. The apparent viscosity predicted by the simulation was in good agreement with previous experimental results. We quantified the deformation of red blood cells as a function of radial position. The numerical results demonstrated that because of the shape transition in response to local shear stress and the wall effect, the radial variation of red blood cell deformation in relatively large microvessels could be classified into three different regions: near-center, middle, and near-wall regions. Effects of the local shear stress and wall varied with vessel diameter, hematocrit, and shear rate.

1. Introduction

Blood is a dense suspension of highly deformable red blood cells (RBCs) in plasma. An RBC is a biconcave cell with a high surface-to-volume ratio, in which a Newtonian solution of hemoglobin is enclosed by a thin membrane. The membrane consists of a lipid bilayer underlined by a spectrin network (Mohandas and Evans, 1994), exhibiting small resistances to shear and bending (Evans, 1983, 1989). Hence, RBCs deform significantly in blood flow. The deformation of RBCs greatly affects the mechanics of blood flow, especially in the microcirculation. Interesting features of blood flow include the Fåhræus effect (Fåhræus, 1929), Fåhræus–Lindqvist effect (Fåhræus and Lindqvist, 1931), and formation of a cell-free layer (CFL) (Goldsmith, 1971; Tateishi et al., 1994; Kim et al., 2007). Recently, it was found that RBC deformation triggers the release of adenosine triphosphate (ATP) (Fischer et al., 2003; Moehlenbrock et al., 2006; Wan et al., 2008; Forsyth et al., 2011), which acts as a signaling molecule in various physiological processes. Some diseases such as malaria (Cooke et al., 2001; Dondorp et al., 2000; Suresh, 2006), type II diabetes (Tsukada et al., 2001), and sickle cell anemia (Higgins et al., 2007) are also linked to RBC deformability. Hence, to better understand the physiological and pathological conditions of the cardiovascular system, it is crucial to quantify the deformation of RBCs.

Recent confocal microscopy with microfluidics has improved experimental measurements of the behavior of RBCs in microvessels. For example, studies have examined the dispersion of RBCs (Lima et al., 2009) and tracer particles (Saadatmand et al., 2011) in 50- to 100-μm vessels using confocal micro-particle tracking velocimetry (Lima et al., 2007). However, owing to light scattering by RBCs and light absorption by hemoglobin, RBCs can be observed only at hematocrits (Hcts) of $<20\%$ with this method (Lima et al., 2009; Saadatmand et al., 2011). Thus, previous experiments have failed to quantify the deformation of RBCs in blood flow at physiologically relevant Hcts.

Numerical modeling can provide information for various Hcts. However, numerical simulations of blood flow in microvessels are challenging because of problems related to coupling membrane mechanics and fluid mechanics as well as computational costs. A few studies have examined three-dimensional simulations of blood flow with multiple RBCs. Zhao et al. (2010) developed a numerical model based on a boundary integral method and analyzed the shapes of RBCs and viscosity for vessels up to 16.9 μm in diameter, involving $O(10^1)$ RBCs. Freund and Orescanin (2011) further investigated the deformation and motion of RBCs, the blood viscosity, and the local Hct in an 11.3-μm vessel using this method. Dupin et al., (2007) proposed a lattice-Boltzmann-based method and simulated $O(10^2)$ RBCs in a rectangular channel. Clausen et al. (2010) developed a lattice-Boltzmann method for simulating $O(10^3)$ RBCs on the IBM Blue Gene/P, but they focused on the performance of their method. Dissipative particle dynamics has also been applied successfully to investigate the apparent viscosity and CFL for vessels up to 40 μm in diameter (Fedosov et al., 2010, 2011a, 2011b).

Thus, the deformation of RBCs in microvessels is not well understood. Given that RBCs are approximately 8 μm in diameter, their flow characteristics in vessels with a few tens of micrometers in diameter may differ from those in smaller microvessels. To efficiently

* Corresponding author. Tel.: +81 22 714 8513; fax: +81 22 795 6959.
E-mail address: yimai@pfsl.mech.tohoku.ac.jp (Y. Imai).

0021-9290/$ - see front matter © 2012 Elsevier Ltd. All rights reserved.
http://dx.doi.org/10.1016/j.jbiomech.2012.08.026

simulate blood flow in large microvessels, thousands of RBCs must be involved. Previously, we developed a numerical model of micro-scale blood flow based on a particle method (Kondo et al., 2009; Imai et al., 2010). This method has been applied successfully to study the microcirculation in malaria infection (Kondo et al., 2009; Imai et al., 2010, 2011) and thrombogenesis (Kamada et al., in press). More recently, we have developed a highly scalable parallel implementation of this method for large-scale studies and we confirmed that our model predicted well the CFL thickness and Fåhræus effect (Alizadehrad et al., 2012). The objective of the present paper was to investigate the deformation of RBCs in microvessels for a variety of vessel diameters, Hcts, and shear rates. We simulated blood flow in circular channels for diameters of 8–50 μm, Hcts of 20–45%, and shear rates of 20–150 s^{-1}. First, our model was further validated by comparing the apparent viscosities between our simulation and experimental results. Then, we quantified the deformation of RBCs for these conditions.

2. Methods

2.1. Numerical model

The details of the model can be found in Imai et al. (2010), and we provide a brief review here. All blood components, including plasma, cytoplasm, and membranes, are modeled using a finite number of particles. Assuming that plasma and cytoplasm are incompressible viscous fluids, the motion of particles is governed by the conservation laws of mass and momentum as

$$\frac{D\rho}{Dt}=0, \tag{1}$$

$$\rho\frac{D\mathbf{u}}{Dt}=-\nabla p+\mu\nabla^2\mathbf{u}+\mathbf{f}, \tag{2}$$

where t refers to the time; ρ, the density; $\mathbf{u}$, the velocity; p, the pressure; μ, the dynamic viscosity; D/Dt, the Lagrangian derivative; and $\mathbf{f}$, the external force. We used the moving particle semi-implicit method (Koshizuka and Oka, 1996) to discretize the governing equations. The RBC is modeled as an initially biconcave cell, consisting of membrane particles and cytoplasm particles. A triangular network of membrane particles is constructed, where neighboring particles are connected by a linear spring to represent the elastic property of RBCs. Bending resistance is also considered between neighboring triangles. Forces generated by the stretching/compression and bending are substituted into the external force term in Eq. (2) for membrane particles only. Note that although membrane viscosity is not explicitly modeled, viscous effects in the membrane are naturally included due to the viscous term of Eq. (2). Because the membrane motion is tracked directly by membrane particles, the no-slip condition at the membrane is satisfied in this procedure. In the previous study (Imai et al., 2010), we confirmed that this model simulates the deformation of single RBCs by optical tweezers stretching (Suresh et al., 2005) and the deformation in shear flow (Cranston et al., 1984) with good accuracy. Note that the deformation of RBCs presented in this paper was within the range validated by these single cell tests. Although aggregation of RBCs is expected to be significant at low shear rates (Reinke et al., 1987), the aggregation was not modeled in the present study to concentrate on the effects of mechanical factors on the deformation.

2.2. Parallel computing

To simulate blood flow in relatively large microvessels with thousands of RBCs, we developed a highly scalable algorithm for parallel computing (Alizadehrad et al., 2012). The computational domain is divided into several sub-domains and distributed among the processors of concurrent parallel processing systems. In this model, the numbering of membrane particles and their network connections are designed in a particular order to minimize communication. Local communication between neighbor processors uses a message-passing interface (MPI) library, including non-blocking communication. In a test for strong scaling, the resulting speed-up increased almost linearly with the number of processors, in which the code was run on Quad-Core Xeon clusters connected with a Gigabit Ethernet.

2.3. Analysis

Consider a straight, circular microvessel with diameter D and length L. The boundary conditions are the no-slip condition at the wall and a periodic boundary condition at the channel inlet and outlet. To drive the flow in the channel, the pressure difference Δp is given between the inlet and the outlet. To avoid the effect of periodic boundary condition, the length is set to be long enough, at least $L/D>2$ and $L/d_{RBC}>8$, where d_{RBC} is the diameter of RBCs, and specifically, $L=66$, 120, 79, and 113 μm for $D=19$, 24, 37 and 50 μm, respectively. The parameters of plasma and RBCs are listed in Table 1. Each simulation is run for sufficient time to remove the effects of the initial transition and data are analyzed over the time at almost quasi-steady state. The flow is characterized by the pseudo-shear rate $\gamma=U/D$, where U is the mean velocity of blood including both plasma and RBCs for the quasi-steady state. Because the velocity of blood is fluctuated in time even at the quasi-steady state, we averaged the velocity for approximately 0.3 s to have the mean velocity U.

Table 1
Parameters for numerical model.

Density of plasma:	ρ_p	1.0×10^3 kg/m^3
Density of cytoplasm:	ρ_c	1.0×10^3 kg/m^3
Viscosity of plasma:	μ_p	1.3×10^{-3} Pa s
Viscosity of cytoplasm:	μ_c	8.0×10^{-3} Pa s
Initial length of spring:	l_0	4.6×10^{-7} m
Stretching spring constant:	k_s	1.0×10^{-5} N/m
Bending spring constant:	k_b	2.4×10^{-11} N

Previously, we confirmed that this model simulated well the thickness of CFL and Fåhræus effect (Alizadehrad et al., 2012) for vessels up to 50 μm. To further validate the numerical results, the apparent viscosity was compared with experimental data. The apparent viscosity of blood in microvessels depends on the vessel diameter and the Hct, which is referred to as Fåhræus–Lindqvist effect (Fåhræus and Lindqvist, 1931). The apparent viscosity is calculated relative to the viscosity of plasma as

$$\frac{\mu_b}{\mu_p}=\frac{Q_p}{Q_b}, \tag{3}$$

where μ_b is the apparent viscosity, and Q_p and Q_b are the respective flow rates for plasma only (without RBCs) and blood. For given values of D, L, μ_p, and Δp, the flow rate Q_p is obtained analytically. The value of the relative apparent viscosity is averaged over the time for a quasi-steady state.

To quantify the deformation of RBCs, the gyration tensor of an RBC is calculated as

$$\mathbf{G}=\frac{1}{M}\sum_{m=1}^{M}(\mathbf{x}_m-\mathbf{x}_g)\otimes(\mathbf{x}_m-\mathbf{x}_g), \tag{4}$$

where $\mathbf{x}_m$ is the position vector of the m-th membrane particle of the RBC, and $\mathbf{x}_g$ is the center of gravity of the RBC (Noguchi and Gompper, 2005; McWhirter et al., 2009; Pan et al., 2010). The gyration tensor is a symmetric 3×3 matrix with three eigenvalues, $\lambda_1\geq\lambda_2\geq\lambda_3$. Assuming that the shape of a stretched RBC is an ellipsoid, the eigenvalues correspond to the diameters, and the stretching ratios can be obtained from

$$s_i=\frac{\sqrt{\lambda_i}-\sqrt{\lambda_i^0}}{\sqrt{\lambda_i^0}}, \tag{5}$$

where λ_i^0 is the i-th eigenvalue at the reference state, and $\lambda_1^0=\lambda_2^0>\lambda_3^0$ for the initial biconcave shape. To study the radial variation in the stretch, $S_i(r)$, the value of s_i is averaged over the space and time, for the RBCs whose center of gravity is located at a radial position within $r\pm1$ μm. We also measure the orientation of the RBCs, where the inclination angle θ is determined by the angle between the eigenvector associated with the eigenvalue λ_3 and the flow direction, *i.e.*, $\theta/\pi=0$ for the orientation perpendicular to the flow and $\theta/\pi=0.5$ for the orientation parallel to the flow.

3. Results and discussion

3.1. Apparent viscosity

The relative apparent viscosity obtained from the simulations is shown in Fig. 1 for vessel diameters ranging from 9 to 50 μm and Hcts of 20%, 30%, and 45%, with a pseudo-shear rate of around 90 s^{-1}. Pries et al. (1992) provided an empirical description of *in vitro* experimental data for the apparent viscosity as a function of the diameter and Hct. Our results agreed very well with their description. Our model correctly reproduced a nonlinear increase in the apparent viscosity with increases in vessel diameter and Hct. While the description by Pries et al. (1992) was based on an averaged apparent viscosity for pseudo-shear rates >50 s^{-1}, it is

known that the apparent viscosity is also affected by the shear rate (Wells and Merrill, 1961; Lipowsky et al., 1980). We examined shear rates of 20 and 150 s^{-1} for diameter of 37 μm and shear rate of 20 s^{-1} for diameter of 50 μm, which are also seen in the microcirculation (Lipowsky et al., 1978). Although the shear rate has a smaller influence than the diameter and Hct, the apparent viscosity decreased as the shear rate increased. With a low Hct (20%) at a diameter of 37 μm, the difference in apparent viscosity was small between the low (20 s^{-1}) and high (150 s^{-1}) shear rates, while with a high Hct (45%), the difference was enhanced. A similar difference in apparent viscosity between shear rates was found for a diameter of 50 μm. In the experimental data of Pries et al. (1992), we can see that a higher Hct allows greater variation in the apparent viscosity. This may reflect a shear rate difference as one of the factors.

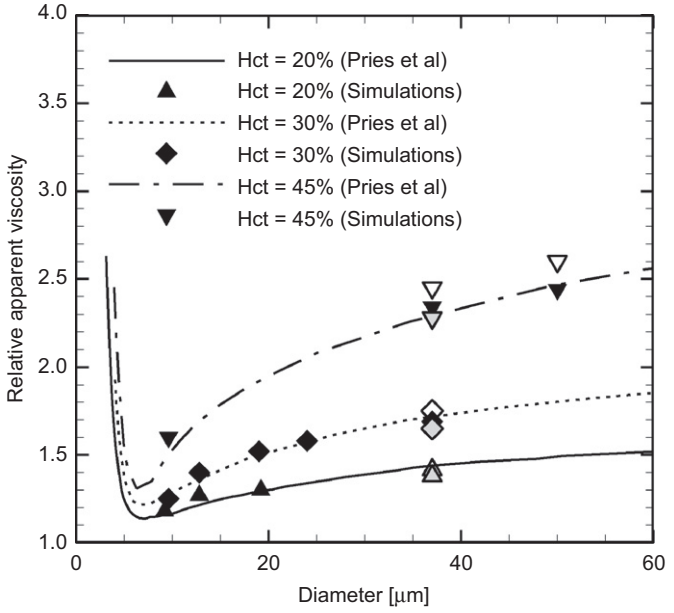

Fig. 1. The relative apparent viscosity μ_b/μ_p as a function of vessel diameter. Simulated results for Hct=20%, 30%, and 45%, and $\gamma=90\pm5$ (black symbols) are compared with experimental results by Pries et al. (1992). Some results for $\gamma=20$ (white symbols) and 150 s^{-1} (grey symbols) are also plotted.

3.2. Deformation of RBCs

Fig. 2a and b shows snapshots of the blood flow for $D=50$ μm and $\gamma=90$ s^{-1}. To visualize the shapes and orientations of RBCs in the center of the vessel, we cut the domain in the central plane of the vessel. Note that it is difficult to obtain such a clear image in experiments due to light absorption by hemoglobin and light scattering by RBCs. General motion of RBCs was a tank-treading motion with the oscillation of inclination angle (swinging motion), and this motion was particularly observed near the wall. The averaged stretching ratios S_1 and S_3, and the inclination angle θ/π are presented in Fig. 2c and d as a function of the radial position r/R, where R is the vessel radius. From these figures, the radial position can be classified into three regions: the near-center, middle, and near-wall regions. In the near-center region, i.e., $r/R<0.2$ ($r<5$ μm), the stretching ratios and inclination angle changed sharply. The small negative value of S_1 and positive value of S_3 at the center of the channel correspond to parachute-shaped RBCs. RBCs in this region were oriented randomly, resulting in a smaller value of θ/π with a larger deviation than in other regions.

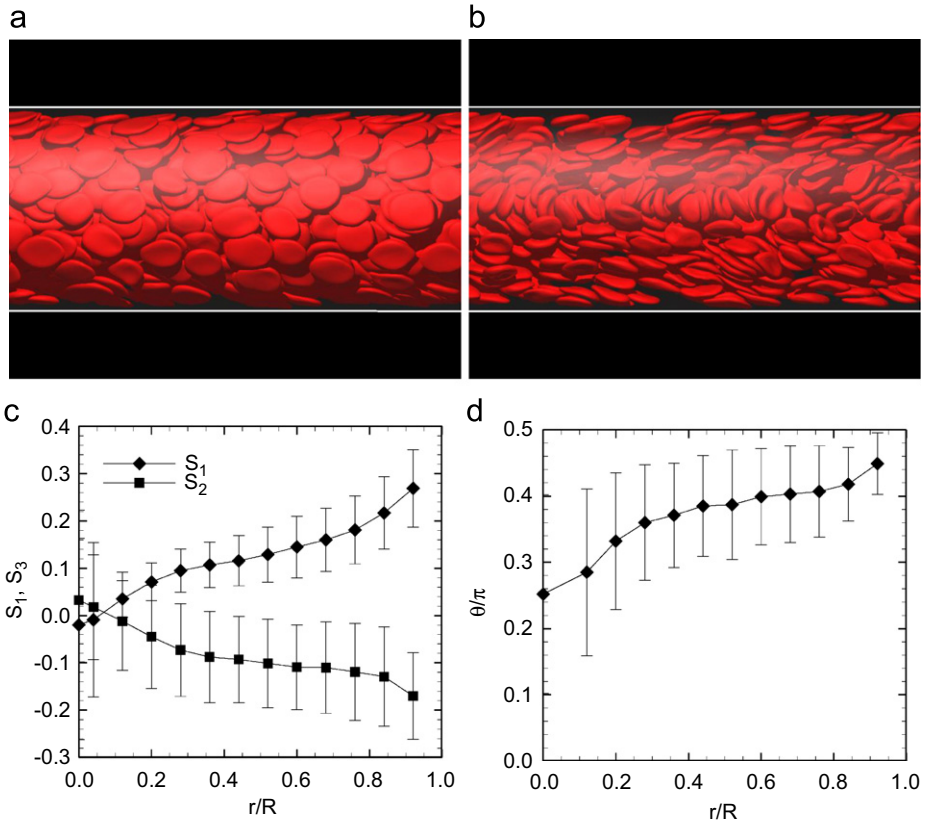

Fig. 2. Numerical results for $D=50$ μm, Hct=45%, and $\gamma=90$ s^{-1}. (a) A snapshot of typical RBCs. (b) The same as (a), but the domain is cut in the central plane of the vessel. (c) The stretching ratios, and (d) inclination angle of RBCs as a function of radial position. The error bars indicate the standard deviation.

As the position approached $r/R=0.2$, the RBCs shifted gradually to disc-like shapes aligned with the flow direction. These shape and orientation shifts caused sharp changes in the stretching ratios and inclination angle. In the middle region, estimated as $0.2<r/R<0.5$ ($5\ \mu m<r<12.5\ \mu m$), the stretching ratio S_1 increased almost linearly, but with a small slope. By contrast, in the near-wall region, $r/R>0.5$ ($r>12.5\ \mu m$), the value of S_1 increased rapidly toward the CFL, while the inclination angle showed a small increase. This is likely due to the trapezoidal velocity profile of the blood flow, in which a significant increase in the local shear rate occurs near the wall, and also due to the wall effect. Hence, in the near-wall region, almost all of the RBCs were highly elongated discs and inclined parallel to the flow direction. As a small change in the radial position markedly alters the local shear rate, the deviation in the stretching ratio was largest for the near-wall region.

3.3. Effects of shear rate, Hct, and vessel size

To investigate the effect of the shear rate on deformation, the stretching ratio S_1 was compared among $\gamma=20$, 95, and $150\ s^{-1}$ for $D=37\ \mu m$ and Hct=30% (Fig. 3a). Fig. 3b and c shows snapshots for $\gamma=20\ s^{-1}$ and $\gamma=150\ s^{-1}$. The general tendency of the radial variation for these cases was the same as for $D=50\ \mu m$ and Hct=45%. However, the response to the shear rate was nonlinear. A change from 20 to $95\ s^{-1}$ caused a large increase in the stretch, whereas the difference in the stretch between 95 and $150\ s^{-1}$ was small, even near the wall. Experimental studies have shown that the deformation of a single RBC exhibits a nonlinear response to the applied shear stress in shear flow conditions (Pfafferott et al., 1985), and similar results were obtained from optical tweezers stretching (Suresh et al., 2005). Therefore, this result may reflect deformation at the single-cell level.

We also examined the effect of the Hct on deformation. We simulated three Hcts, Hct=20, 30, and 45%, for $D=37\ \mu m$, with a pseudo-shear rate of approximately $95\ s^{-1}$. As shown in Fig. 4a, the stretch ratio S_1 did not differ significantly among the Hct values in the near-center region. The stretch was slightly greater at higher Hcts, particularly in the near-wall region. This effect can be explained by the velocity profile and CFL thickness. As the Hct increases, the plug flow profile near the center becomes more prominent, resulting in a higher shear rate near the wall for a

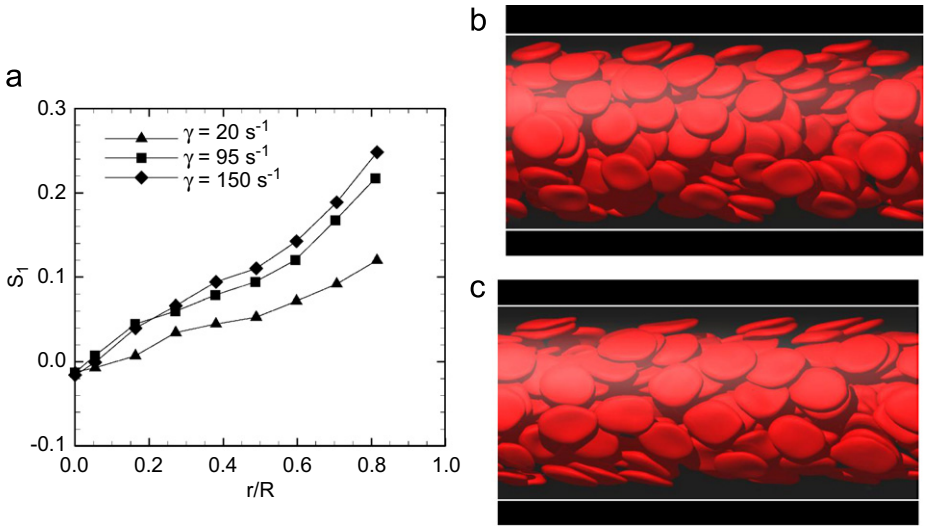

Fig. 3. (a) Comparison of the stretching ratio S_1 among different pseudo-shear rates γ, for Hct=30% and $D=37\ \mu m$. Snapshots of the blood flow for (b) $\gamma=20\ s^{-1}$ and (c) $\gamma=150\ s^{-1}$.

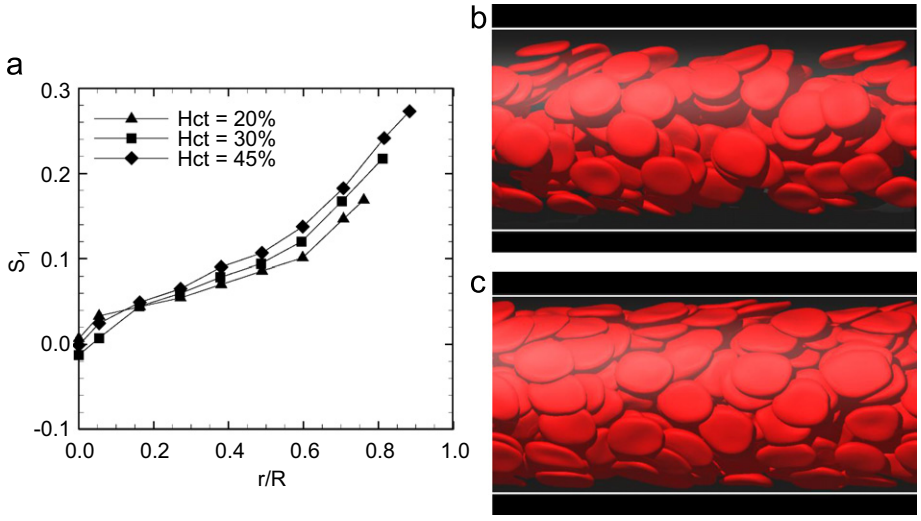

Fig. 4. (a) Comparison of the stretching ratio S_1 among different Hcts, for $\gamma=95\ s^{-1}$ and $D=37\ \mu m$. Snapshots of the blood flow for (b) Hct=20% and (c) Hct=45%.

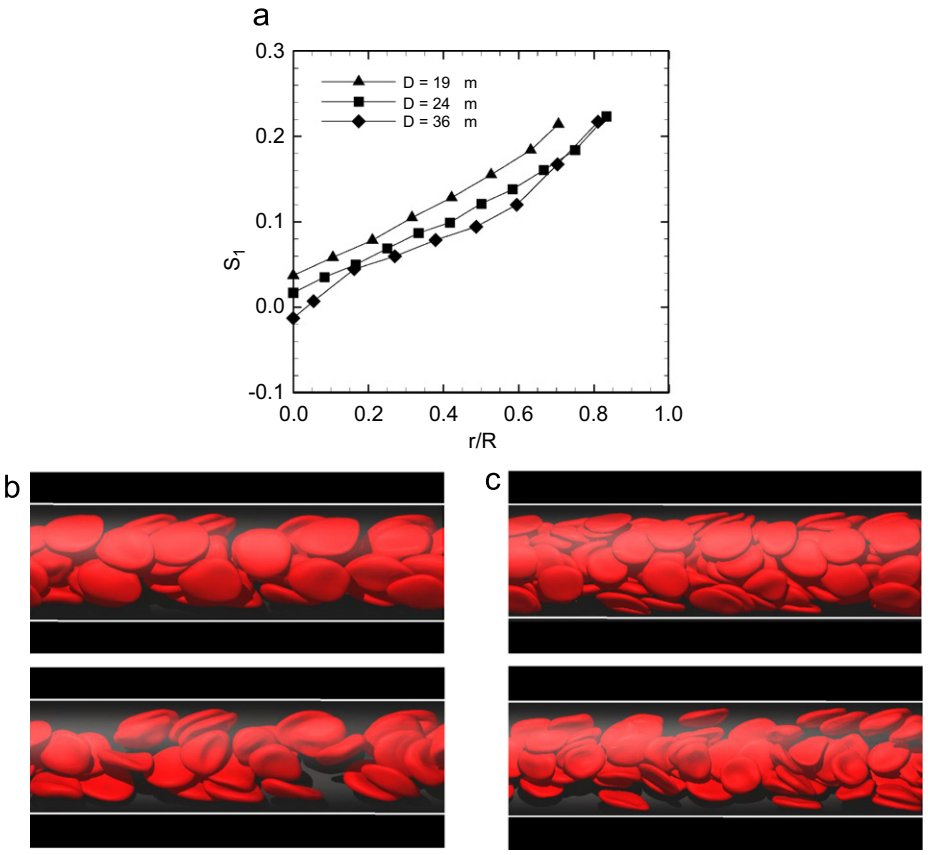

Fig. 5. Comparison among vessels with different diameters for Hct=30% and $\gamma=95\pm5\ s^{-1}$. (a) Stretching ratio S_1. Snapshots of RBCs for (b) $D=19\ \mu m$ and (c) $D=24\ \mu m$. The domains are cut at the center plane of the vessels in the lower images.

fixed pseudo-shear rate. This was confirmed by the corresponding snapshots (Fig. 4b and c). At a higher Hct, the CFL thickness, *i.e.*, the RBC distance from the wall, decreases; consequently, RBCs in the near-wall region are exposed to higher shear stress.

To assess how the radial variation in the stretch changes in smaller vessels, we analyzed $D=19$, 24, and 37 μm with Hct=30%, where $\gamma=95\pm5\ s^{-1}$ for all cases. Note that RBCs flow in single file and form a parachute-like shape in further small vessels such as $D=8\ \mu m$. It is obvious that such small vessels has no radial variation and shows the near-center region only. However for $D=19$ and 24 μm, the near-center region was not found (Fig. 5a). As shown in Fig. 5b and c, the parachute-shaped RBCs almost all disappeared, particularly for $D=19\ \mu m$. RBCs tended to deform into disc-like shapes aligned with the flow direction. This RBC shape and orientation are similar to the results for $D=16.9\ \mu m$ presented by Zhao et al. (2010). Although the border between the middle and near-wall regions was somewhat vague, the stretch also showed a nonlinear increase near the CFL for $D=19$ and 24 μm. The wall effect may be extended farther inside a small vessel than a large vessel. This may cause an unclear border between these regions, and a greater stretch in the middle region.

4. Conclusions

A parallel simulation of a particle-based model has been applied to study RBCs deformation in microvessels. The predicted apparent viscosity was in good agreement with experimental data, and this result supports the validity of our model. To our knowledge, this is the first quantitative study of the deformation of RBCs in vessels with a few tens of micrometers in diameter. Our simulation demonstrated that because of the shape transition in response to local shear stress and the wall effect, the radial variation in deformation can be classified into three regions: the near-center, middle, and near-wall regions. The influence of these factors varied with vessel diameter, hematocrit, and shear rate. These results should help to further understand the mechanics of blood flow and mass transport in microvessels, for example ATP release is induced by the deformation of RBCs. Some diseases such as malaria and sickle cell anemia are linked to a reduction in RBC deformability. In a future study, it will be interesting to clarify the relationship between RBC deformation and blood flow mechanics in these diseases.

Conflicts of interest statement

There is no conflict of interest.

Acknowledgments

This research was supported by a Grant-in-Aid for Scientific Research (S) (No. 23220012), by a Grant-in-Aid for Young Scientists (A) (No. 24680048) from the JSPS.

References

Alizadehrad, D., Imai, Y., Nakaaki, K., Ishikawa, T., Yamaguchi, T., 2012. Parallel simulation of cellular flow in microvessels using a particle method. Journal of Biomechanical Science and Engineering 7, 57–71.

Clausen, J.R., Reasor, D.A., Aidun, C.K., 2010. Parallel performance of a lattice-Boltzmann/finite element cellular blood flow solver on the IBM Blue Gene/P architecture. Computer Physics Communications 181, 1013–1020.
Cooke, B.M., Mohandas, N., Coppel, R.L., 2001. The malaria-infected red blood cell: structural and functional changes. Advances in Parasitology 50, 1–86.
Cranston, H.A., Boylan, C.W., Carroll, G.L., Sutera, S.P., Williamson, J.R., Gluzman, I.Y., Krogstad, D.J., 1984. *Plasmodium falciparum* maturation abolishes physiologic red cell deformability. Science 223, 400–403.
Dondorp, A.M., Vreeken, K.J., White, N.J., 2000. Abnormal blood flow and red blood cell deformability in severe malaria. Parasitology Today 16, 228–232.
Dupin, M.M., Halliday, I., Care, C.M., Alboul, L., Munn, L.L., 2007. Modeling the flow of dense suspensions of deformable particles in three dimensions. Physical Review E 75, 066707.
Evans, E.A., 1983. Bending elastic modulus of red blood cell membrane derived from buckling instability in micropipette aspiration tests. Biophysical Journal 43, 27–30.
Evans, E.A., 1989. Structure and deformation properties of red blood cells: concepts and quantitative methods. Methods in Enzymology 173, 3–35.
Fåhræus, R., 1929. The suspension stability of the blood. Physiological Reviews 9, 241–274.
Fåhræus, R., Lindqvist, T., 1931. The viscosity of the blood in narrow capillary tubes. American Journal of Physiology 96, 562–568.
Fedosov, D.A., Caswell, B., Popel, A.S., Karniadakis, G.E., 2010. Blood flow and cell-free layer in microvessels. Microcirculation 17, 615–628.
Fedosov, D.A., Pan, W., Caswell, B., Gompper, G., Karniadakis, G.E., 2011a. Predicting human blood viscosity in silico. Proceedings of the National Academy of Sciences of the United States of America 108, 11772–11777.
Fedosov, D.A., Caswell, B., Suresh, S., Karniadakis, G.E., 2011b. Quantifying the biophysical characteristics of *Plasmodium-falciparum*-parasitized red blood cells in microcirculation. Proceedings of the National Academy of Sciences of the United States of America 108, 35–39.
Fischer, D.J., Torrence, N.J., Sprung, R.J., Spence, D.M., 2003. Determination of erythrocyte deformability and its correlation to cellular ATP release using microbore tubing with diameters that approximate resistance vessels in vivo. Analyst 128, v1163–v1168.
Forsyth, A.M., Wan, J., Owrutsky, P.D., Abkarian, M., Stone, H.A., 2011. Multiscale approach to link red blood cell dynamics, shear viscosity, and ATP release. Proceedings of the National Academy of Sciences of the United States of America 108, 10986–10991.
Freund, J.B., Orescanin, M.M., 2011. Cellular flow in a small blood vessel. Journal of Fluid Mechanics 671, 466–490.
Goldsmith, H.L., 1971. Red cell motions and wall interactions in tube flow. Federation Proceedings 30, 1578–1590.
Higgins, J.M., Eddington, D.T., Bhatia, S.N., Mahadevan, L., 2007. Sickle cell vasoocclusion and rescue in a microfluidic device. Proceedings of the National Academy of Sciences of the United States of America 104, 20496–20500.
Imai, Y., Kondo, H., Ishikawa, T., Yamaguchi, T., 2010. Modeling of hemodynamics arising from malaria infection. Journal of Biomechanics 43, 1386–1393.
Imai, Y., Nakaaki, K., Kondo, H., Ishikawa, T., Lim, C.T., Yamaguchi, T., 2011. Margination of red blood cells infected by *Plasmodium falciparum* in a microvessel. Journal of Biomechanics 44, 1553–1558.
Kamada, H., Imai, Y., Nakamura, M., Ishikawa, T., Yamaguchi, T. Computational analysis on the mechanical interaction between a thrombus and red blood cells: possible causes of membrane damage of red blood cells at microvessels. Medical Engineering and Physics, http://dx.doi.org/10.1016/j.medengphy.2012.01.003, in press.
Kim, S., Kong, R.L., Popel, A.S., Intaglietta, M., Johnson, P.C., 2007. Temporal and spatial variations of cell-free layer width in arterioles. American Journal of Physiology Heart and Circulatory Physiology 293, H1526–H1535.
Kondo, H., Imai, Y., Ishikawa, T., Tsubota, K., Yamaguchi, T., 2009. Hemodynamic analysis of microcirculation in malaria infection. Annals of Biomedical Engineering 37, 702–709.
Koshizuka, S., Oka, Y., 1996. Moving-particle semi-implicit method for fragmentation of incompressible fluid. Nuclear Science and Engineering 123, 421–434.
Lima, R., Ishikawa, T., Imai, Y., Takeda, M., Wada, S., Yamaguchi, T., 2009. Measurement of individual red blood cell motions under high hematocrit conditions using a confocal micro-PTV system. Annals of Biomedical Engineering 37, 1546–1559.
Lima, R., Wada, S., Takeda, M., Tsubota, K., Yamaguchi, T., 2007. In vitro confocal micro-PIV measurements of blood flow in a square microchannel: the effect of the haematocrit on instantaneous velocity profiles. Journal of Biomechanics 40, 2752–2757.
Lipowsky, H.H., Kovalcheck, S., Zweifach, B.W., 1978. The distribution of blood rheological parameters in the microvasculature of cat mesentery. Circulation Research 43, 738–749.
Lipowsky, H.H., Usami, S., Chien, S., 1980. In vivo measurements of "apparent viscosity" and microvessel hematocrit in the mesentery of the cat. Microvascular Research 19, 297–319.
McWhirter, J.L., Noguchi, H., Gompper, G., 2009. Flow-induced clustering and alignment of vesicles and red blood cells in microcapillaries. Proceedings of the National Academy of Sciences of the United States of America 106, 6039–6043.
Moehlenbrock, M.J., Price, A.K., Martin, R.S., 2006. Use of microchip-based hydrodynamic focusing to measure the deformation-induced release of ATP from erythrocytes. Analyst 131, 930–937.
Mohandas, N., Evans, E., 1994. Mechanical properties of the red cell membrane in relation to molecular structure and genetic defects. Annual Review of Biophysics and Biomolecular Structure 23, 787–818.
Noguchi, H., Gompper, G., 2005. Shape transitions of fluid vesicles and red blood cells in capillary flows. Proceedings of the National Academy of Sciences of the United States of America 102, 14159–14164.
Pan, W., Caswell, B., Karniadakis, G.E., 2010. A low-dimensional model for the red blood cell. Soft Matter 6, 4366–4376.
Pfafferott, C., Nash, G.B., Meiselman, H.J., 1985. Red blood cell deformation in shear flow. Effects of internal and external phase viscosity and of in vivo aging. Biophysical Journal 47, 695–704.
Pries, A.R., Neuhaus, D., Gaehtgens, P., 1992. Blood viscosity in tube flow: dependence on diameter and hematocrit. American Journal of Physiology Heart and Circulatory Physiology 263, H1770–H1778.
Reinke, W., Gaehtgens, P., Johnson, P.C., 1987. Blood viscosity in small tubes: effect of shear rate, aggregation, and sedimentation. American Journal of Physiology Heart and Circulatory Physiology 253, H540–H547.
Saadatmand, M., Ishikawa, T., Matsuki, N., Abdekhodaie, M.J., Imai, Y., Ueno, H., Yamaguchi, T., 2011. Fluid particle diffusion through high-hematocrit blood flow within a capillary tube. Journal of Biomechanics 44, 170–175.
Suresh, S., Spatz, J., Mills, J.P., Micoulet, A., Dao, M., Lim, C.T., Beil, M., Seufferlein, T., 2005. Connection between single-cell biomechanics and human disease states: gastrointestinal cancer and malaria. Acta Biomaterialia 1, 15–30.
Suresh, S., 2006. Mechanical response of human red blood cells in health and disease: some structure–property–function relationships. Journal of Materials Research 21, 1871–1877.
Tateishi, N., Suzuki, Y., Soutani, M., Maeda, N., 1994. Flow dynamics of erythrocytes in microvessels of isolated rabbit mesentery: cell-free layer and flow resistance. Journal of Biomechanics 27, 1119–1125.
Tsukada, K., Sekizuka, E., Oshio, C., Minamitani, H., 2001. Direct measurement of erythrocyte deformability in diabetes mellitus with a transparent microchannel capillary model and high-speed video camera system. Microvascular Research 61, 231–239.
Wan, J., Ristenpart, W.D., Stone, H.A., 2008. Dynamics of shear-induced ATP release from red blood cells. Proceedings of the National Academy of Sciences of the United States of America 105, 16432–16437.
Wells, R.E.J., Merrill, E.W., 1961. Shear rate dependence of the viscosity of whole blood and plasma. Science 133, 763–764.
Zhao, H., Isfahani, A.H.G., Olson, L.N., Freund, J.B., 2010. A spectral boundary integral method for flowing blood cells. Journal of Computational Physics 229, 3726–3744.